SVOA Materials Science & Technology

ISSN: 2634-5331

ScienceVolks Open Access

Research Article

Assessment of Stress Corrosion Cracking Behavior of Additively Processed Al-Mg-Sc-Zr Alloy

A.B. Spierings*[1], K. Kern[2], Y. Steimer[2], F. Palm[3] and K. Wegener[4]

Affiliation:

[1]*Innovation Centre for Additive Manufacturing, INSPIRE-AG, Fürstenlandstrasse 122 , CH-9014 St. Gallen, Switzerland*

[2]*Materials Engineering, Eastern Switzerland University of Applied Sciences, Werdenbergstrasse 4, CH-9471 Buchs, Switzerland*

[3]*Airbus Central Research & Technology, XRXS, Willy Messerschmittstrasse 1, D-82024 Taufkirchen, Germany*

[4]*Institute of Machine Tools and Manufacturing, Department of Mechanical and Process Engineering, ETH Zurich, CH-8092 Zurich, Switzerland*

***Corresponding Author:** A.B. Spierings, Innovation Centre for Additive Manufacturing, INSPIRE-AG, Fürstenlandstrasse 122 , CH-9014 St. Gallen, Switzerland*

***Received:** March 12, 2021 **Published:** April 05, 2021*

Abstract:

Additively manufactured (AM) structures provide significant advantages in terms of lightweight engineering potentials, using methods like topology optimization or the integration of lattice structures. Applications in automotive, aerospace and space therefore require high-strength aluminum alloys, for which structural 2xxx, 5xxx, 6xxx or 7xxx alloys are applied. Scalmalloy is a newer Sc- and Zr- modified hardenable high-strength Al-Mg alloy, offering very good mechanical properties. However, from an industrial perspective not only the mechanical properties are of importance, since structural parts are also exposed to chloride environmental conditions, leading to corrosion effects. It is therefore mandatory to characterize the corrosion behavior. In this respect the corrosion behavior of additively processed Al-alloys have so far mostly been characterized for AlSi10Mg alloys using electrochemical potential analysis methods, while the experimental testing of stress corrosion properties has not been reported. The study analyzed the stress corrosion cracking susceptibility of a Al-Mg-Sc-Zr alloy processed by Selective Laser Melting. The results indicate that the AM-processed Al-Mg-Sc-Zr alloy shows at least moderate stress corrosion resistance according to the ECSS-standard, even though the microstructural situation in such welded materials is different to conventionally processed materials.

Keywords: Laser Powder Bed Fusion, Aluminum, Stress corrosion cracking, ECSS standard, space requirements

1. Introduction

Additive manufacturing (AM) technologies and specifically the Laser Powder Bed Fusion (LPBF-) process (more commonly known as the Selective Laser Melting, SLM) is gaining interest for structural applications in various industrial sectors, including automotive, aerospace and space. In this process, a thin powder layer is selectively scanned by a high-power laser beam, to locally melt and consolidate the powder material in the regions where a part is built. Various alloys can be processed achieving very good properties, such as almost 100% density associated with very good mechanical properties. An overview on typical materials is given by Frazier [11] and Kok et al. [19]. This layer-by-layer manufacturing process enables the manufacture of very complex geometries, such as topology optimized structures, lightweight parts with integrated lattice structures and/or with increased functional integration. In this respect, Mouriaux and Berkau [27] demonstrated the manufacture of a topology optimized aluminium antenna bracket for satellite applications, achieving a significant weight reduction of 40% compared to a traditional design, together with an increased stiffness by 30%.

Aluminium alloys are of special interest for lightweight applications. Currently, 4xxx alloys are the most often processed alloys due to their near eutectic composition, and specifically the properties of the LPBF-processed hardenable variant AlSi10Mg have been investigated in detail [3, 6, 9, 43-45]. However, there is a significant need for Al-alloys better suitable for structural applications, for which 2xxx, 5xxx, 6xxx and 7xxx high-strength alloys can be potential candidates, even though these alloys are known to be difficult to be processed due to their solidification cracking susceptibility [1].

There is therefore an increasing trend for the development of alloy formulations specifically designed for the LPBF-process, to achieve optimal processing conditions and material properties. A review on such alloy developments is given by Aversa et al. [1]. One promising alternative to casting alloys is the Scalmalloy material, being a Sc- an Zr-modified Al-Mg alloy, which offers Sc-based precipitation hardening capabilities leading to very good mechanical properties. Spierings et al. [37] report yield strength > 480MPa and ultimate strength > 520MPa in the heat treated condition, while Schmidke et al. [33] report even slightly higher values. Therefore, such an alloy is especially suitable for structural applications in space and aerospace [33]. The alloy furthermore displays an advantageous microstructure. Spierings et al. [36] and other researchers [2] investigated microstructrual features and formation principles and found a bi-modal microstructure with an extremly very fine grained region with sub-micron sized equiaxed grains next to slightly larger columnar grains. This supports the reduction of anisotropic mechanical properties, which is typical for most other AM-processed materials, as shown exemplarily by Merten et al. [26], Hitzler et al. [15, 16] and Tang et al. [43].

However, from an industrial perspective, next to attractive mechanical properties the corrosion behavior of materials is of outmost importance, since structural parts in aerospace, space and automotive are also exposed to demanding environmental conditions. In this respect, the corrosion behavior of wrought or cast Al-alloys is widely documented. Gahli [12] summarizes that the passivity of aluminium depends on the protective oxide film, having a thickness of only a few nanometers at room temperature. According to the Pourbaix diagram, this amorphous passive film is only produced in a pH range between 4 and 9. On the other hand, the corrosion behavior of AM-processed alloys is only very rarely investigated, while differences to their conventionally processed counterparts can be expected due to significant microstructural differences. Sander et al. [32] summarized potential effects of AM process variables and their influence on the corrosion susceptibility for a number of alloys. It becomes clear that the refined microstructure of AM-processed materials as a result of the very high cooling rates during processing leads to a heavily increased density of grain boundaries. Since Gahli [12] reports that stress corrosion cracking (SCC) in aluminium alloys is typically characterized by intergranular corrosion, SCC could be promoted in such alloys. On the other hand, the complex processing conditions during LPBF are characterized by rapid solidification, partial re-melting, and a cyclic heat treatment, which can lead to different precipitation behavior, and related phases. Therefore, the types of phases, their sizes and volumetric densities could also affect the local corrosion behavior, as they act based on their electrochemical potentials with respect to the Al matrix.

The corrosion behavior of LPBF-processed Al-alloys is only rarely investigated. While Sander et al. [32] reviewed in total 8 publications mostly on AlSi10Mg, a summary for the general discussion is given here. Gharbi et al. [13] investigated the electrochemical potentials of an as-processed LPBF-AA2024 alloy, and reported a distinct shift in the pitting potenial, which was attributed to the absence of the S-phase, while only minimal changes in the cathodic polarisation response were observed. In addition dissolution profiles measured in 0.01M NaCl revealed that the Al corrosion rate for the additively processed alloy was about 5 times lower than the T3-heat treated conventional counterpart, as a result of the formation of a thicker Al-oxide film. They concluded that the AM-processed material displayed an improved corrosion resistance, even though further work will be necessary to better understand AM-processed Al-alloy dissolution behavior. Cabrini et al. [5] investigated the corrosion behavior of as-processed AlSi10Mg in an aerated diluted Harrison solution using potentiodynamic testing and electrochemical impedance spectroscopy, and characterized the behavior for different build orientations, and polished and blasted surface finishs. They found preferential dissolution of -Al at the melt-pool border where grain sizes are known to be very small [25, 45, 46], and where grains are decorated by Si particles. This higher Si concentration gives rise to higher corrosion rates in these areas. The result was confirmed by Revilla et al. [28], who related the corrosion rates with the cellular grain size and the potential differences between -Al and Si. Furthermore, a slight dependency on sample orientation was found by Cabrini et al. [5], with higher corrosion rates at surfaces parallel to the build direction, which was also attributed to the high density of melt-pool borders with a correspondingly fine grained microstructure. Polished surfaces displayed a better corrosion resistance, however, shot peened surfaces display some lower residual porosities, which themselves are preferential sites for local corrosion. Hence, the local corrosion current density and pitting potential depends on the numbers and dimensions of these surface-open porosities. Leon et al. [22] also investigated the effect of the surface roughness on the corrosion resistance under LCF conditions in a 3.5% NaCl solution. They reported that the as-processed rough surfaces result in lower corrosion resistance compared to polished samples, and explained this by the relatively large amount of cavities and other process-related surface defects, which is basically in-line with the finding of Cabrini et al. [5]. The effect of a heat treatment on AlSi10Mg was investigated by Cabrini et al. [4], where they found that a low temperature stress relieve did not reduce the susceptibility to penetrating selective attack. However, a high temperature heat treatment, which leads to the precipitation of larger Si-particles with a correspondingly higher electrochemical potential led to localized corrosion, but without any penetrating selective attack.

Since this paper deals with the corrosion resistance of Sc- and Zr- containing Al-Mg alloys, some reference to the properties of these alloys are made. Røyset and Ryum [31] reviewed the effects of Sc and summarize that it seems that Sc slightly increases the corrosion potential of an Al-alloy, and makes it therefore somewhat more noble. An effect that takes place especially at hypereutectic compositions when primary or eutectic Al3Sc-precipitates contribute to the potential, and therefore also the heat treatment can affect the corrosion potential. While the corrosion potential is not descriptive for the self-corrosion resistance of an alloy, it seems that when Sc is added to wrought Al-alloys, the corrosion resistance is considerably improved. Røyset states that Al-Mg-Sc alloys were highly resistant to SCC, even though other references refer to the fact that mircogalvanic corrosion next to Al3Sc particles may take place. Li et al. [24] analysed the stress corrosion susceptibility of cast, heat treated Al–Zn–Mg alloys that were modified with Sc concentrations of 0.06 wt% and 0.11 wt%.

They found that the grain boundary Al3Sc-precipitates help to minimize recrystallization, which improves stress corrosion resistance, as also stated by Røyset. However, the effect of grain boundary precipitates on corrosion resistance was mainly active at the low Sc-concentration, while at the higher concentration the effect was superimposed by the higher electrochemical activity of precipitates, which then led to an increase in SCC susceptibility.

There is only few literatures available on the corrosion behavior of LPBF-processed Sc- and Zr- modified Al-Mg alloys. Li et al. [23] studied the electrochemical corrosion behavior of a LPBF-processed Sc and Zr modified Al-6.2 Mg alloy in a 3.5% NaCl solution using potentiodynamic polarization. They report higher corrosion resistance for higher laser energy densities, potentially due to reduced residual material defects. Furthermore, the absence of anodic and cathodic active surface reduced the susceptibility to corrosion, while also the rapid solidification, which prevents Al3Sc dissolution, resulted in higher corrosion resistance. They conclude that the electrochemical corrosion properties of the LPBF alloy variant are even better compared to the cast counterpart. Recently, Gu et al. [14] published their results of electrochemcial and microstructural analysis of a similar LPBF-processed Al-4.2Mg-0.4Sc-0.2Zr alloy. They performed electrochemical studies on its corrosion behavour in a 3.5% NaCl solution, and with a special focus on the effect of the different microstructures given in the xy-build plane, and the xz-plane parallel to the build direction using polished surfaces. The results indicated that the xy-plane exhibits a better corrosion resistance compared to the xz-plane, for which factors such as precipitations, different grain size distributions, grain misorientation angles and crystallographic orientations were considered. They found that the xy-planes possess higher electrochemical potentials, lower corrosion current densities and higher polarization resistance values compared to the xz-planes. Hence, xy-planes display somewhat better corrosion resistance for pitting initiation. The passive behavior is confirmed for both plane orientations, mainly Al2O3 and Al (OH)3. Polarization tests revealed wide and shallow pits formed on the xy-plane, while on the xz-plance less but deeper pits were generated. They discussed a mechanism for this anisotropic corrosion behavior, where at an early stage a passive film is generated. Once it is broken down Al3(Sc, Zr) precipitates act as local cathodes and promote the propagation of pits. It is therefore reasonable to expect some anisotropic corrosion behavior as the precipiation density and grain sizes, and by that also the grain boundary densities, respectively, are different for the two plane orientations.

It can be concluded that the Sc-concentration in Al-Mg alloys, and the heat treatment procedures and microstructural conditions severly affect the corrosion resistance, for which there are no general rules. It is therefore mandatory to experimentally assess the corrosion behavior of an alloy. So far no assessment of the stress corrosion cracking behavior of LPBF-processed Sc-modified Al-Mg alloy has been reported, even though differences to conventionally processed materials can be expected as the LPBF -process specific material properties may affect the SCC resistance.

1.1 Stress corrosion cracking in 5xxx Al-alloys

Stress corrosion cracking (SCC) in Al-alloys depends on various factors, including the matrix alloy composition and the corresponding volatilization of alloying elements including solute hydrogen, micro-segregation effects from processing sequences, the precipitation of phases and their corrosion potential to the matrix, the microstructure and grain sizes (and by this also recrystallization effects), and finally the corrosive environment where a part is used in and where especially chloride ions from salty environments are drivers for corrosion.

According to Korb and Olson [21] cast 5xxx alloys have a high corrosion resistance, especially if the Mg content is < 3 wt%, and when it remains in solid solution, or is finely distributed in form of Al8Mg5 precipitates throughout the matrix. However, for higher content and if these anodic precipitates are intergranular sitting at grain boundaries, alloys may be more susceptible to exfoliation or stress corrosion cracking, as in aluminum the SCC-paths are intergranular, hence follow the grain boundaries [41]. As a consequence, for such age hardenable alloys, the heat treatment and precipitation of intermetallic phases typically increases SCC susceptibility.

Since in LPBF-processed materials residual material defects such as pores and small cracks are evident, these sites could in combination with an external load act as SCC initiation sites, and further increase the SCC sensitivity. Furthermore, the cyclic heat treatment during LPBF-processing and any post-process heat treatment could lead to unfavourable precipitation of intermetallic phases that also could affect SCC susceptibility. Finally, the tendency for non-equiaxed (columnar) grain formation in AM-processed materials could result in an anisotropic SCC sensitivity. This grain size dependency is also known for wrought aluminum as reported by Gahli [12] and is a result of the different number of stressed grain boundaries.

This paper experimentally investigates the SCC sensitivity of a LPBF-processed Sc- and Zr- modified Al-Mg alloy, known as Scalmalloy, and discusses the corrosion effects. It provides valuable data for the industrial use of LPBF-processed Sc- and Zr- modified Al-Mg alloys.

2. Methods and Materials

2.1 SCC sample production

To manufacture stress corrosion cracking samples by LPBF, Scalmalloy powder material with nominal composition of Al4.6Mg 0.66Sc 0.42Zr 0.49Mn (numbers in wt-%) was used in a ConceptLaser M2 machine equipped with a 200 W fibre laser. A layer thickness t = 30 m and a laser power P = 200 W was used, with a hatch spacing d = 135 m and a scan speed vs = 300 mms^{-1}. The standard ConceptLaser chess-board like scanning strategy was used with an island size of 5 mm x 5 mm, being rotated by 90° from layer to layer, and moved in x- and y-direction by 1mm. The processing parameters result in a volumetric energy density EV = 135 Jmm^{-3} according to equation 1.

$$E_V = \frac{P}{d \cdot t \cdot v_s} \quad (1)$$

The development of this processing window is discussed in more detail in Spierings et al. [34]. Cube samples, produced together with the SSC samples, achieved a mean density of 99.4 ± 0.1% displaying a typical LPBF-processed material density.

Tensile samples according to DIN 50'125-B6x30 with a length of 60mm were used for Stress Corrosion Cracking experiments. This geometry is different to the specimen suggested by the ECSS standard [10], which represents the testing reference. However, the standard allows different sample geometries if the gauge length is at least 10mm, which is fulfilled by the samples used. This change of sample geometry was due to the very long standard ECSS specimen (170 mm or 180 mm), which would require a huge amount of powder material. Hence, to optimize manufacturing costs, the smaller DIN-samples were chosen.

Cylindrical raw samples were manufactured in a horizontal and vertical build orientation, to account for the different microstructural grain orientations in the weld line with respect to the load direction during SCC testing. These samples were subsequently turned to the final geometry (Figure 1, left) achieving a surface quality of at least N6 (Ra=0.8 m). The influence of the as-built surface quality was assessed by the manufacture of vertical samples having the correct sample geometry, and where only the threads were made conventionally (Figure 1, right). The as-built surfaces were finally blasted using an IEPCO MicroPeen blasting device using steel particles (SR0.2B) for a first blasting operation followed by a finishing blasting with ZrO2 powder to further smoothen the surface.

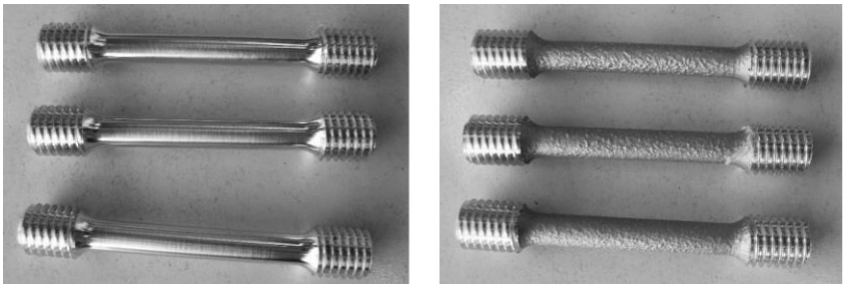

Figure 1: *SCC tensile samples. Left: Turned. Right: As-built and blasted surface quality.*

SCC samples were measured in the as-built condition, hence without a post-process heat treatment, and in a HIPed and heat treated condition (> 1'000 bar @ 325°C / 4h). For each configuration (build orientation and condition) 3 specimens were prepared. The final sample finishing preparation conducted before the SCC test procedure (chapter 2.2) included a degreasing step, followed by a chemical etching procedure according to DIN-17'611 [8]. It was an etching in NaOH solution at a temperature between 50°C and 65°C for about 10min. The samples were then washed in water, followed by a cleaning step with nitric acid. This etching procedure leads to a small material removal between 5 m to 10 m.

2.2 SCC testing

Testing for stress corrosion cracking susceptibility was performed according to the procedure and requirements of the European Cooperation for Space Standardization ECSS, referred to the ECSS-Q-ST-70-37C standard [10]. The standard covers constant-load stress-corrosion testing also for welded Al-materials. The test uses stressed and unstressed control specimens, where the stressed samples were loaded to 75% proof stress referring to Spierings et al. [37, 38]. The samples were exposed to a 3.5% sodium chloride solution at a pH value between 6.4 and 7.2, and for a duration of 30 days. The environmental conditions during the immersion were a temperature of 24°C ± 1°C at 45% ± 10% relative humidity.

2.3 Assessment of stress-corrosion susceptibility

According to ECSS-Q-ST-70-37C standard [10] the susceptibility to stress corrosion is assessed based on the comparison of tensile strength between stressed and unstressed control samples. Tensile testing was performed on a Walter&Bai hydraulic tensile testing machine LFV-25. A clip-on axial extensometer MFA 25 was used having a gauge length of 25 mm. Testing was performed in accordance with EN-10002 / ISO-6892 [18]. From the measured "engineering" stress-strain curves (,) gained from quasi-static tensile testing, the true (index 'T') stress-strain curves and true ultimate strength (Rm,T) is calculated for the plastic region according to Hosford [17], following equation 2, with the elongation from the stress-strain curve.

$$R_{m,T} = R_m \cdot (1 + \varepsilon) \quad (2)$$

The susceptibility is assessed by comparing tensile strengths Rm,T of stressed and unstressed specimens, and by metallographic examination of micrographs. The micrographs were taken from embedded and polished cross-sections taken in the transversal and longitudinal direction of the tensile samples. A Zeiss Axioskop 2MAT microscope was used to capture images at 50x magnification. Following to the ECSS standard, the following classification for stress-corrosion resistance is used:

Table 1: SCC resistance classification according to ECSS-Q-ST-70-37C [10]

Resistance to SCC	Class 1 – high	Class 2 – moderate	Class 3 – low
Fractures during 30 days exposure	None out of three samples		Any of the three stress-corrosion specimens fails
$\overline{R_{m,stressed}} / \overline{R_{m,unstressed}}$	≥ 0.9		< 0.9
metallographic examination	no evidence of stress-corrosion	evidence of stress-corrosion in any of the three stress-corrosion specimens	shows evidence of stress-corrosion

2.4 SEM and EDX analysis

The Zeiss Leo 1455 VP scanning electron microscope (SEM) equipped with a Bruker Roentec Quantax Q400 EDX detector served to image the corroded surface of the tensile testing specimens. The pictures and analysis were done with an acceleration voltage of 20kV in high vacuum mode.

3. Results and Discussion

3.1 Tensile testing of SSC samples

The true ultimate strength values Rm, T for vertically and horizontally built and turned samples in the as-processed and HIPed condition are shown in Figure 2.

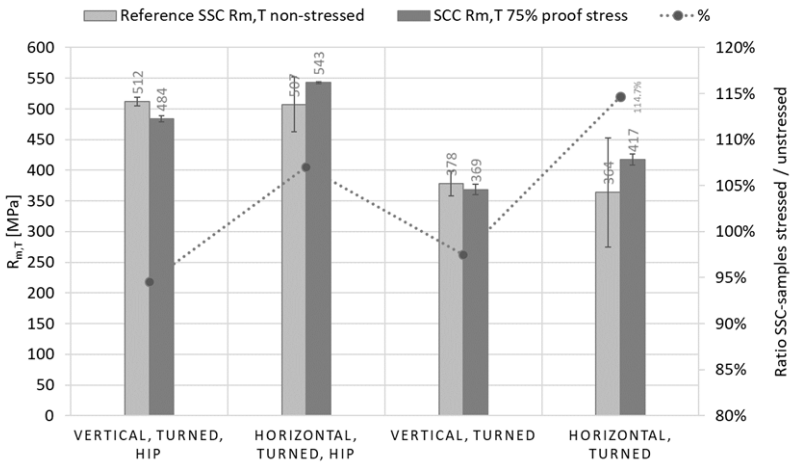

Figure 2: *Ultimate strengths for stressed and unstressed control SSC-specimens for horizontal and vertical build orientations, in the as-built and HIPed condition and turned surfaces. The 2nd axis shows the ratio between stressed and unstressed $R_{m,T}$ values.*

As expected, the material strengths of the HIPed samples is significantly higher (+37%) compared to the as-processed samples. The differences between the horizontal and vertical build orientations are comparably small, as discussed in Spierings et al. [37], and which remains also for the SCC-exposed samples. The differences in Rm, T between stressed and unstressed control samples is also small; their ratios are 94.5% and 107% and fulfil therefore the requirements for class 1 or class 2 resistance (Table 1). The > 100% value refers to the fact that only 3 samples were measured, and that one horizontally built, turned and HIPed sample fractured at a 13% lower Rm, T value compare to the mean of the other two samples ("outlier"). Removing this outlier would results in a ratio of 102%.

Figure 3 shows the results for the vertically built samples with the blasted surface quality in the as-processed and HIPed condition. Thereby, the unstressed blasted samples displayed a 6% higher strength in the HIPed condition, while in the as-processed condition the difference is +8%. This trend for higher mechanical strength on blasted samples could also be observed for standard samples that were not immersed in NaCl-solution, and is explained by the surface-near pre-compression that was achieved by the blasting operation.

The differences in Rm, T between blasted and turned surfaces are only statistically significant for HIPed samples in the unstressed control group ($p > 0.01$), with somewhat higher strength values for the blasted samples this accounts also true for non-immersed standard samples. For non-HIPed as-well as for stressed samples the differences are statistically significant.

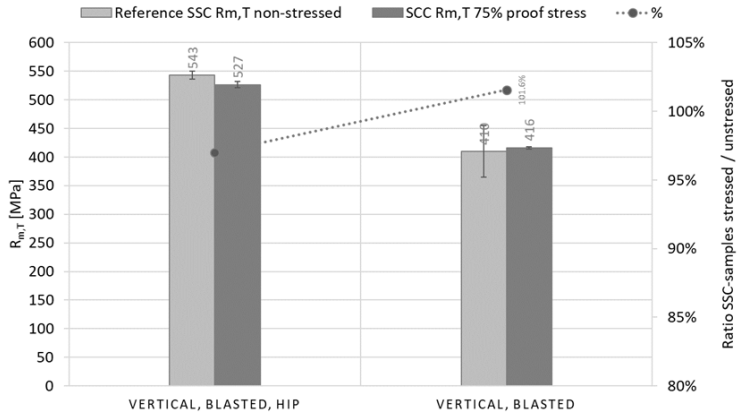

Figure 3: *Ultimate strengths for stressed and unstressed control SSC-specimens for vertical build orientation and as-built surfaces, in the as-built and HIPed condition.*

With regard to stress corrosion the comparison of the stressed and unstressed control samples turns out that the differences are statistically not significant (blasted: $p = 0.065$, blasted HIP: $p = 0.081$), achieving corresponding ratios > 90% (Figure 3), and a quality class 1 or 2.

3.2 Micrographic examination

Figure 4 and Table 2 to Table 4 show micrographs for the 3 material and surface conditions for the vertical and horizontal build orientation. Thereby, the xy-cross-section refers to the xy-build plane. For horizontally built samples, the xy-cross-section is therefore parallel to the long-axis of the tensile samples, while this plane is perpendicular to the axis for vertically built samples. Figure 4 displays micrographs in the xy- and the xz-plane at a 50x magnification. It shows that corrosion on surfaces occasionally takes place. According to the requirements of the ECSS standard [10] micrographs at higher magnification (500x) shown in Table 2 to Table 4 were taken at such specific locations of interest, to characterize potential corrosion attack.

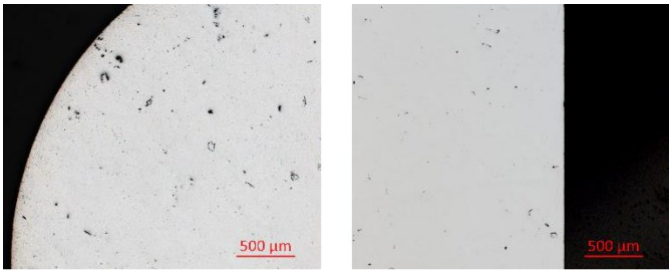

Figure 4: *xy-micrograph (left) and xz-mircograph (right) from as-built, turned and stressed sample.*

The micrographs shown in Table 2 summarize local corrosion attack for stressed and unstressed, HIPed samples manufactured in the horizontal and vertical orientation, and with a turned surface quality. Small corrosion-related defects are obvious, with a typical depth ≤ 50 m. There was no intergranular grain boundary related corrosion detected, but a more pitting-like corrosion of the surface. No significant differences between stressed and unstressed control samples can be observed.

Table 2: Micrographs for HIPed and turned samples in the horizontal and vertical build orientation. Scale bar = 50 m.

	HIP - Vertical build orientation		HIP - Horizontal build orientation	
	xy	xz	xz	xy
turned control	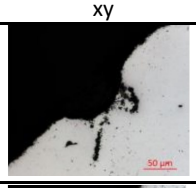	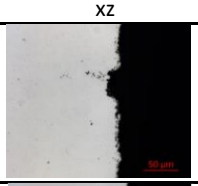	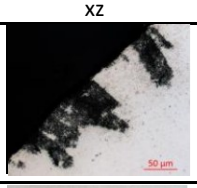	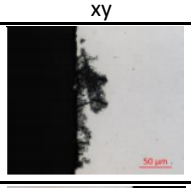
turned stressed	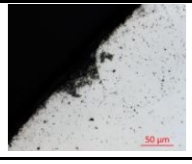		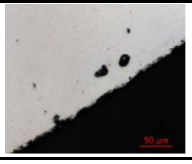	

Table 3 shows the micrographs for the as-built material condition, for horizontal and vertical build orientation and turned surfaces for both the stressed and unstressed control samples. Next so some increased internal porosity, surface near corrosion partially took place, while there is a slight indication that corrosion seems to penetrate some deeper into the material. This effect could be related to this increased level of residual porosity in the material that favors a faster penetration of corrosion attack into the material. However, after the 30 days of exposure, penetration depths still were smaller than approximately 100 m.

Table 3: Micrographs for as-built and turned samples in the horizontal and vertical build orientation. Scale bar = 50 m.

	As built - Vertical build orientation		As built - Horizontal build orientation	
	xy	xz	xz	xy
turned control		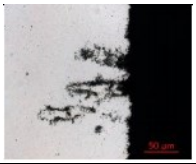	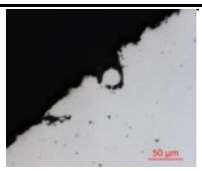	
turned stressed	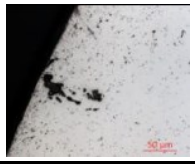		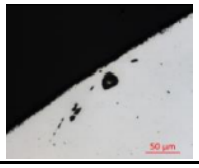	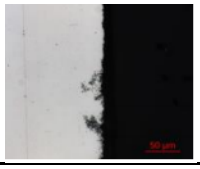

The corrosion behavior for the blasted stressed and unstressed samples for both build orientations are shown Table 4.

Some regions of plastic deformation from the blasting operation can be observed, leading to an increased density of surface-near cavities. These cavities can promote corrosion attack deeper into the material, and consequently corrosion attack distances reach values up to about 150 m to 200 m into the material, while no significant differences can be observed between stressed and unstressed samples.

Table 4: Micrographs for as-built and blasted samples in the vertical build orientation. Scale bar = 50 m.

	HIP - Vertical build orientation		As-built - Vertical build orientation	
	xy	xz	xy	xz
blasted control	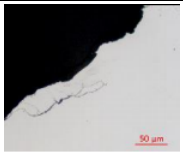	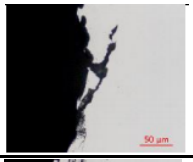	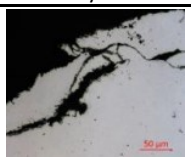	
blasted control	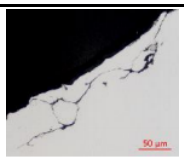	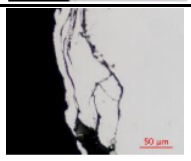	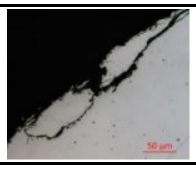	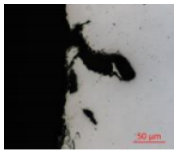

The figures in Table 4 show small surface-near channels, which are expected to be the result of the plastic deformation of surface adhering powder particles by the blasting operation. Such channels can further promote crevice corrosion effects [7], and lead to stress concentration that could potentially affect the mechanical performance. However, the results from Figure 3 show basically no significant further influence of corrosion on the mechanical performance. Even when compared to non-SCC reference samples [37], no significant effect of the blasting operation on the mechanical performance could be observed, which is expected to be the result of the surface-near compression state that is achieved by the blasting operation. However, from the figures in Table 4 it seems that the corrosion effects are some more pronounced. It can therefore be expected that the presence of such channels could lead to some higher corrosion effects at longer exposure durations, as observed by Leon et al. [22] for AlSi10Mg.

3.3 SEM-EDX surface examination

In order to analyze the corrosion phenomena, SEM examinations of surfaces of horizontally built samples in the following conditions are performed: HIPed/turned, as-built/turned and as-built/blasted surfaces.

Figure 5b shows the SEM-BSD magnification of a HIPed and turned sample. Most of the surface remained unaffected by corrosion, and represents the typical base material as discussed by Spierings et al. [35]. The base material seems not very prone to corrosion, as there is a common understanding that a Sc-addition to Al-alloys improves the self-corrosion resistance in general, as summarized by Røyset and Ryum [31]. Some corrosion phenomena however can be observed on all specimens: Localized corrosion, visible on the samples as greyish areas predominately rich in O and Cl, and pitting like local corrosion attack at embedded particles with typical sizes of 20 m to 40 m. These particles are of more complex composition, as indicated by the EDX analysis in Figure 5, and are rich in Ni, Mn, Cr and Co. The higher electron densities of these elements (compared to the aluminium alloy) yields a stronger back scattering of electrons and therefore these regions appear brighter in SEM-BSD magnification in Figure 5b.

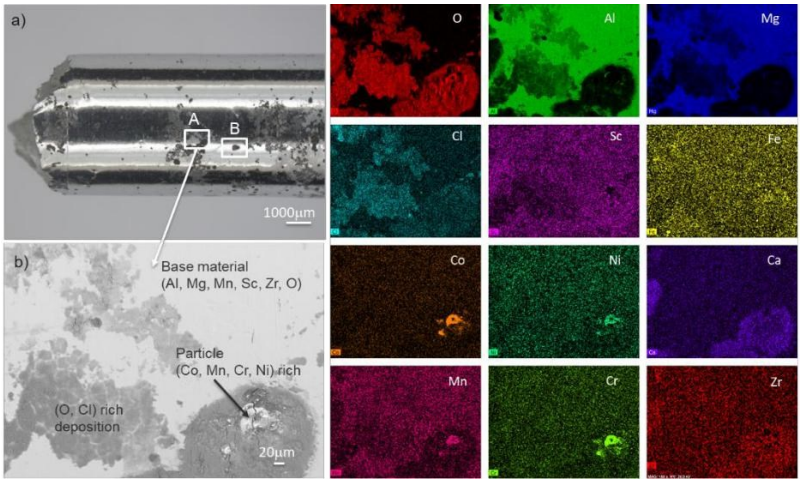

***Figure 5**: a) HIPed/turned sample surfaces with selected analysed areas A and B. b) SEM (BSD) magnification and EDX elemental mapping of area A showing the base material, plate-like O- and Cl-rich areas and a particle with complex elemental composition.*

Such embedded particles as the one shown in Figure 5b display a specific corrosion potential to the base material and lead therefore to local corrosion effects in the vicinity of these particles. It is unclear where these particles come from. One possible source could be the LPBF machine used, if the build chamber and/or recoating system were not properly cleaned from the powders of previous build jobs. This however is considered unlikely, since the machine components were carefully cleaned with Ethanol. It seems more likely that these particles source back to the process chain used for the production of the experimental powder material, and where for example remaining powder particles from sieving operations can potentially lead to such a contamination. This however could also happen during powder recycling after LPBF build jobs.

Figure 6 shows details of the pitting-like corrosion area B from Figure 5a. The magnification in Figure 6b shows a typical corrosion attack as it is known for Al-alloys. The metal is susceptible to the formation of pits in the vicinity of second phase particles or impurities which are cathodic to the matrix and therefore lead to its localized accelerated dissolution [7, 40]. The corroded area is rich in elements of the base material, next to O and Cl. The Oxygen is present in the base material from oxidized powder material, and together with Cl also sources from the sodium chloride (NaCl-) solution. Within area B very small, light, embedded Ni-rich particles in a size range of typically < 5 m are visible. It is expected that such particles also promote pitting corrosion as in Figure 6, due to a higher concentration of corrosion products. The source of such small particles is unknown, but could be the same as discussed above. However, while typical particle sizes in LPBF powders are at least about a factor of 2 to 10 larger than these particles are [39, 42], it is more likely that such particles source back to the gas- and filter system used in LPBF machines, and might be blown into the processing chamber during operation.

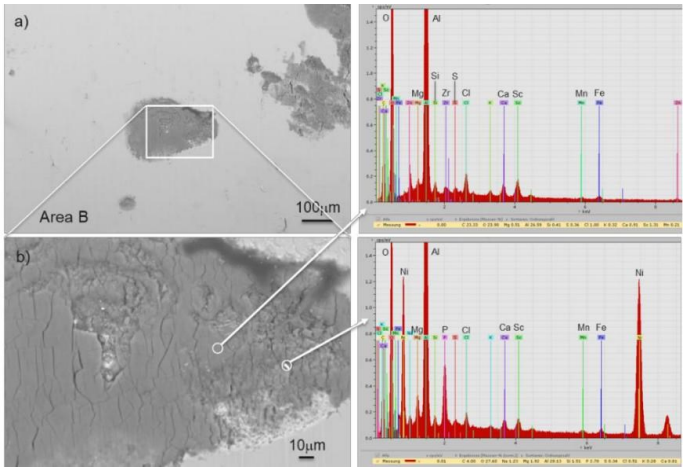

***Figure 6**: a) Area B from Figure 5 with selected pitting-like corrosion region shown in b). EDX composition analysis for the pitting region and for a small Ni-rich particle*

Figure 7a displays the corroded surface of an as-built and turned sample, where pitting corrosion covers a significant amount of the surface. From the appearance the corrosion is basically identical to the one on HIPed samples, but much more pronounced, potentially due to the higher amount of open pores from the as-built material condition (see also Table 3). Such pores favor the progress of localized corrosion effects, leading to a visually heavily attacked surface that is covered by corrosion products (Figure 7a) as described for LPBF specimens with a higher surface roughness [20, 29]. Similar to Figure 5b a contamination particle with complex composition promotes the corrosion, while this particle is composed of various metals (Ni, Co, Fe, Cr), and also Ti. Since the LPBF machine was only very rarely used with Ti, it is expected that such particles source from the powder production route.

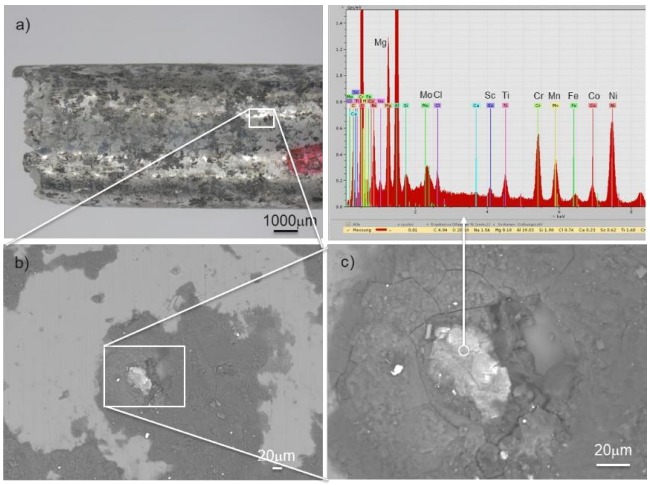

Figure 7*: a) As-built/turned sample surface with selected analysed area shown in b) and c). EDX composition analysis for the particle with complex composition with Ni, Co, Cr, Mn and Ti.*

An even more pronounced corrosion attack is shown in Figure 8a on as-process/blasted surfaces, where the surface shows plated structures (see also Table 4) that promote corrosion effects similar to open porosity (Figure 7), but in a higher intensity. Comparable to the previous material conditions, very fine, bright particles (Figure 8b) but also larger particles were found on these surfaces as-well.

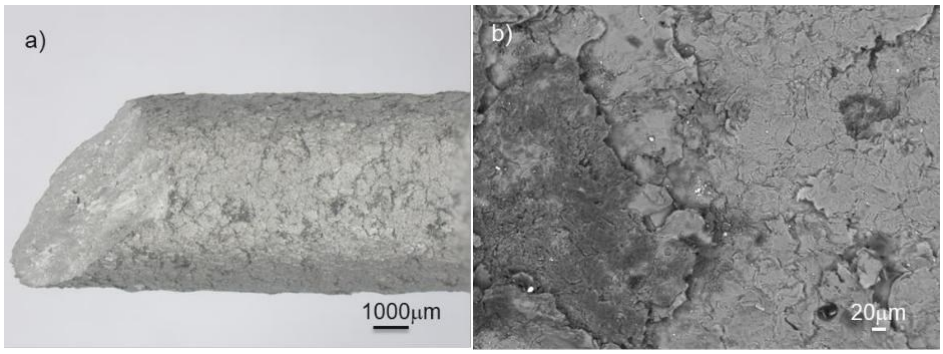

Figure 8*: a) As-built/blasted sample surface. B) SEM (BSD) magnification showing plate like surface structure from the blasting process*

4. Conclusion

Stress corrosion cracking experiments were conducted on LPBF-processed Al-Mg-Sc-Zr-Mn alloy, known as Scalmalloy. It can be concluded that the material generally displays a good stress corrosion resistance, which is in-line with the statements of Røyset and Ryum [31]. The absence of Si in the alloy, together with the fine dispersed coherent Al3Sc precipiates limit the corrosion susceptibility, even though some corrosion effects can be observed on the sample surfaces. These types are a pitting-like corrosion, potentially driven by the more porous microstructure of the unHIPed material.In addition material contaminations in the form of particle inclusions of various compositions can act as local micro-galvanic corrosion points. Also fine particles in the low m-range were found that act in a similar way.

The experiments result in the following main conclusions.

- Pitting-like surface corrosion takes place, while the HIPed material condition shows the least corrosion attack, followed by the as-processed material condition due to some higher open porosity. The highest corrosion attack was found on as-processed/blasted condition due to a high amount of open porosity and cavities.
- Material contamination in the form of large and fine particles of various compositions were found, potentially from the powder manufacturing process and/or previous LPBF build jobs. Such particles promote local corrosion due to a higher corrosion potential.

- Even though corrosion effects take place, it is mainly an esthetic problem. The mechanical performance of stressed SCC samples is ≥ 90% of the unstressed control samples of any condition: Horizontal and vertical build orientation, as-processed and HIPed material, and turned and blasted surface quality. According to the ECSS-Q-ST-70-37C standard [10], the LPBF-processed Scalmalloy reaches moderate class-2 stress corrosion cracking resistance.
- Neither the mechanical properties nor the micrographic examination of the stressed samples showed susceptibility of the material to stress corrosion cracking. Nevertheless it is generally recommended to avoid any material contamination to minimize corrosion effects.

The results therefore approve the use of AM-processed Scalmalloy products for space- and aerospace applications.

Conflict of Interest

The authors declare no conflict of interest.

Acknowledgements

The authors gratefully acknowledge Mr. M. Demont for supporting the production of samples and mechanical material analysis.

Funding

This work was partially supported by the Swiss Commission for Technology and Innovation (CTI) [grant number 17365.1].

References

1. Aversa A, Marchese G, Saboori A, Bassini E, Manfredi D, Biamino S, Ugues D, Fino P, Lombardi M (2019) New Aluminum Alloys Specifically Designed for Laser Powder Bed Fusion: A Review. *Materials*, 12(7): p. 1007.
2. Awd M, Tenkamp J, Hirtler M, Siddique S, Bambach M, Walther F (2018) Comparison of Microstructure and Mechanical Properties of Scalmalloy® Produced by Selective Laser Melting and Laser Metal Deposition. Materials, 11(1): p. 17.
3. Buchbinder D, Schleifenbaum H, Heidrich S, Meiners W, Bültmann J (2011) High Power Selective Laser Melting (HP SLM) of Aluminum Parts. *Physics Procedia*, 12, Part A(0): p. 271-278.
4. Cabrini M, Lorenzi S, Pastore T, Pellegrini S, Ambrosio EP, Calignano F, Manfredi D, Pavese M, Fino P (2016) Effect of heat treatment on corrosion resistance of DMLS AlSi10Mg alloy. *Electrochimica Acta*, 206: p. 346-355.
5. Cabrini M, Lorenzi S, Pastore T, Pellegrini S, Manfredi D, Fino P, Biamino S, Badini C (2016) Evaluation of corrosion resistance of Al–10Si–Mg alloy obtained by means of Direct Metal Laser Sintering. *Journal of Materials Processing Technology*, 231: p. 326-335.
6. Chen B, Moon SK, Yao X, Bi G, Shen J, Umeda J, Kondoh K (2017) Strength and strain hardening of a selective laser melted AlSi10Mg alloy. *Scripta Materialia*, 141: p. 45-49.
7. de la Fuente D (2020) Corrosion of Aluminum, Aluminum Alloys, and Composites, in *Reference Module in Materials Science and Materials Engineering*. Elsevier. p. 1-9.
8. DIN (2000) *Anodized products of wrought aluminium and wrought aluminium alloys*, in *DIN 17611*. DIN German Institute for Standardization. p. 11.
9. Domfang Ngnekou JN, Nadot Y, Henaff G, Nicolai J, Kan WH, Cairney JM, Ridosz L (2019) Fatigue properties of AlSi10Mg produced by Additive Layer Manufacturing. *International Journal of Fatigue*, 119: p. 160-172.
10. European_Space_Agency (2008) *Space product assurance ECSS-Q-ST-70-37C*, in *Determination of the susceptibility of metals to stress-corrosion cracking*. ESA-ESTEC: Noordwijk, The Netherlands. p. 31.
11. Frazier W (2014) Metal Additive Manufacturing: A Review. *Journal of Materials Engineering and Performance*, 23(6): p. 1917-1928.
12. Gahli E (2011) Uhlig's Corrosion Handbook, in *The Electrochemical Society Series*, R. Winston Revie, Editor. John Wiley & Sons, Inc.: Hoboken, New Jersey. p. 1285.
13. Gharbi O, Jiang D, Feenstra DR, Kairy SK, Wu Y, Hutchinson CR, Birbilis N (2018) On the corrosion of additively manufactured aluminium alloy AA2024 prepared by selective laser melting. *Corrosion Science*, 143: p. 93-106.
14. Gu D, Zhang H, Dai D, Ma C, Zhang H, Li Y, Li S (2020) Anisotropic corrosion behavior of Sc and Zr modified Al-Mg alloy produced by selective laser melting. *Corrosion Science*, 170: p. 108657.
15. Hitzler L, Janousch C, Schanz J, Merkel M, Heine B, Mack F, Öchsner A (2017) Direction and Location dependency of Selective Laser Melted AlSi10Mg Specimens. *J. Mater. Process. Technol.*, 243: p. 48-61.

16. Hitzler L, Sert E, Schuch E, Öchsner A, Merkel M, Heine B, Werner E (2020) Fracture toughness of L-PBF fabricated aluminium-silicon: A quantitative study on the directional dependency of the crack tip to the layering. *Progress in Additive Manufacturing*, in submission.

17. Hosford WF (2005) *Mechanical Behavior of Materials*. New York: Cambridge University Press. 447.ISO-6892-1 (2009) *ISO 6892-1: Metallic materials - Tensile testing - Part 1: Method of test at room temperature* ISO Standards International. p. 61.

18. Mertens AI, Delahaye J, Lecomte-Beckers J (2017) Fusion-Based Additive Manufacturing for Processing Aluminum Alloys: State-of-the-Art and Challenges. *Adv. Eng. Mater.*, (1700003): p. 13.

19. Kok Y, Tan XP, Wang P, Nai MLS, Loh NH, Liu E, Tor SB (2018) Anisotropy and heterogeneity of microstructure and mechanical properties in metal additive manufacturing: A critical review. *Materials & Design*, 139: p. 565-586.

20. Kong D, Dong C, Ni X, Li X (2019) Corrosion of metallic materials fabricated by selective laser melting. *npj Materials Degradation*, 3(1): p. 24.

21. Korb LJ, Olson DL (1987) *ASM Metals HandBook Volume 13 Corrosion*. Metals Handbook. Vol. 13. ASM International. p. 3455.

22. Leon A, Aghion E (2017) Effect of surface roughness on corrosion fatigue performance of AlSi10Mg alloy produced by Selective Laser Melting (SLM). *Materials Characterization*, 131: p. 188-194.

23. Li R, Wang M, Yuan T, Song B, Chen C, Zhou K, Cao P (2017) Selective laser melting of a novel Sc and Zr modified Al-6.2Mg alloy: Processing, microstructure, and properties. *Powder Technology*, 319: p. 117-128.

24. Li Z, Jiang H, Wang Y, Zhang D, Yan D, Rong L (2018) Effect of minor Sc addition on microstructure and stress corrosion cracking behavior of medium strength Al–Zn–Mg alloy. *Journal of Materials Science & Technology*, 34(7): p. 1172 -1179.

25. Manfredi D, Calignano F, Krishnan M, Canali R, Ambrosio EP, Atzeni E (2013) From Powders to Dense Metal Parts: Characterization of a Commercial AlSiMg Alloy processed through Direct Metal Laser Sintering. *Materials*, 6: p. 856-869.

26. Mertens AI, Delahaye J, Lecomte-Beckers J (2017) Fusion-Based Additive Manufacturing for Processing Aluminum Alloys: State-of-the-Art and Challenges. Adv. Eng. Mater., (1700003): p. 13.

27. Mouriaux F, Berkau A (2016) *Certified for Universal Success: Additive Manufacturing of Satellite Components*. EOS, Krailling-Munich, Germany. p. 3.

28. Revilla RI, Liang J, Godet S, De Graevea I (2017) Local Corrosion Behavior of Additive Manufactured AlSiMg AlloyAssessed by SEM and SKPFM. *Journal of The Electrochemical Society*, 164(2): p. 27-35.

29. Revilla RI, Verkens D, Rubben T, De Graeve I (2020)Corrosion and Corrosion Protection of Additively Manufactured Aluminium Alloys-A Critical Review. *Materials (Basel, Switzerland)*, 13,DOI:10.3390/ma13214804.

30. Røyset J (2007) Scandium in Aluminium Alloys Overview: Physical metallurgy, Properties and Applications.*Metallurgical Science and Technoology*, 25(2): p. 11-21.

31. Røyset J, Ryum N (2005) Scandium in aluminium alloys. *Int. Mater. Rev.*, 50(1): p. 19-44.

32. Sander G, Tan J, Balan P, Gharbi O, Feenstra DR, Singer L, Thomas S, Kelly RG, Scully JR, Birbilis N (2018) Corrosion of Additively Manufactured Alloys: A Review. *Corrosion*, 74 (12): p. 1318-1350.

33. Schmidtke K, Palm F, Hawkins A, Emmelmann C (2011) Process and Mechanical Properties: Applicability of a Scandium modified Al-alloy for Laser Additive Manufacturing. *Phys. Procedia*, 12(Part 1): p. 369-374.

34. Spierings AB (2018) *Powder spreadability and characterization of Sc- and Zr-modified aluminium alloys processed by Selective Laser Melting - Quality management system for additive manufacturing*, in *Institute of Machine Tools and Manufacturing*. ETHZ, PhD Nr. 24721: Zurich. p. 256.

35. Spierings AB, Dawson K, Dumitraschkewitz P, Pogatscher S, Wegener K (2018) Microstructure characterization of SLM-processed Al-Mg-Sc-Zr alloy in the heat treated and HIPed condition. *Additive Manufacturing*, 20: p. 173-181.

36. Spierings AB, Dawson K, Heeling T, Uggowitzer PJ, Schäublin R, Palm F, Wegener K (2017) Microstructural features of Sc- and Zr-modified Al-Mg alloys processed by selective laser melting. *Mater. Des.*, 115: p. 52-63.

37. Spierings AB, Dawson K, Kern K, Palm F, Wegener K (2017) SLM-processed Sc- and Zr-modified Al-Mg alloy: Mechanical properties and microstructural effects of heat-treatment. *Materials Science & Engineering A*, 701: p. 264-273.

38. Spierings AB, Dawson K, Voegtlin M, Palm F, Uggowitzer PJ (2016) Microstructure and mechanical properties of as-processed Scandium-modified aluminium using Selective Laser Melting. *CIRP Ann. Manuf. Technol.*, 65(1): p. 213-216.

39. Spierings AB, Herres N, Levy G (2011) Influence of the particle size distribution on surface quality and mechanical properties in additive manufactured stainless steel parts. Rapid Prototyping Journal, 17(3): p. 195 - 202.

40. Szklarska-Smialowska Z (1999) Pitting corrosion of aluminum. Corrosion Science, 41(9): p. 1743-1767.

41. Szklarska-Smialowska Z (1999) Pitting corrosion of aluminum. Corrosion Science, 41(9): p. 1743-1767.

42. Tan JH, Wong WLE, Dalgarno KW (2017) An overview of powder granulometry on feedstock and part performance in the selective laser melting process. *Additive Manufacturing*, 18: p. 228-255.

43. Tang M, Pistorius PC (2017) Anisotropic mechanical behaviour of AlSi10Mg Parts produced by Selective Laser Melting. *JOM*, 69(3): p. 516-522.

44. Tang M, Pistorius PC (2017) Oxides, porosity and fatigue performance of AlSi10Mg parts produced by selective laser melting. *International Journal of Fatigue*, 94(2): p. 192-201.

45. Thijs L, Kempen K, Kruth J-P, Van Humbeeck J (2013) Fine-structured aluminium products with controllable texture by selective laser melting of pre-alloyed AlSi10Mg powder. *Acta Materialia*, 61(5): p. 1809-1819.

46. Trevisan F, Calignano F, Lorusso M, Pakkanen J, Aversa A, Ambrosio EP, Lombardi M, Fino P, Manfredi D (2017) On the Selective Laser Melting (SLM) of the AlSi10Mg Alloy: Process, Microstructure, and Mechanical Properties. *Materi-*

Citation: A.B. Spierings, K. Kern, Y. Steimer, F. Palm and K. Wegener. "Assessment of Stress Corrosion Cracking Behavior of Additively Processed Al-Mg-Sc-Zr Alloy". SVOA Materials Science &Technology, 2021, 3(2) Pages: 24-35.